J|A|C|S ARTICLES

Published on Web 11/18/2010

Structure-Induced Ferromagnetic Stabilization in Free-Standing Hexagonal $Fe_{1.3}Ge$ Nanowires

Hana Yoon,[†] Alex Taekyung Lee,[‡] Eun-Ae Choi,[‡] Kwanyong Seo,[†] Nitin Bagkar,[†] Jaehun Cho,[§] Younghun Jo,[§] K. J. Chang,*[,‡] and Bongsoo Kim*[,†]

Department of Chemistry, and Department of Physics, KAIST, Daejeon 305-701, Korea, and Division of Materials Science, KBSI, Daejeon 305-333, Korea

Received May 15, 2010; E-mail: bongsoo@kaist.ac.kr; kchang@kaist.ac.kr

Abstract: Single-crystalline free-standing hexagonal $Fe_{1.3}Ge$ nanowires (NWs) are synthesized for the first time using a chemical vapor transport process without using any catalyst. Interestingly, $Fe_{1.3}Ge$ NWs are found to be ferromagnetic at room temperature, while bulk $Fe_{1.3}Ge$ has the lower critical temperature of 200 K. We perform first-principles density functional calculations and suggest that the observed strong ferromagnetism is attributed to the reduced distances between Fe atoms, increased number of Fe−Fe bonds, and the enhanced Fe magnetic moments. Both experimental and theoretical studies show that the magnetic moments are enhanced in the NWs, as compared to bulk $Fe_{1.3}Ge$. We also modulate the composition ratio of as-grown iron germanide NWs by adjusting experimental conditions. It is shown that uniaxial strain on the hexagonal plane also enhances the ferromagnetic stability.

One-dimensional (1D) nanowires (NWs) have unique electronic, optical, and mechanical properties as a result of their dimensional anisotropy and the quantum confinement effect.[1] Free-standing NWs that are ferromagnetic above room temperature have attracted much attention for practical applications in the field of nanospintronics.[2,3]

Ferromagnetic transition-metal and group IV semiconductor alloy NWs such as CoSi[3a] and Fe_5Si_3[3b] attract particular interest, as they are compatible with existing complementary metal−oxide−semiconductor (CMOS) technologies and thus can be integrated into future nanospintronic devices.[3] While transition-metal silicide NWs have been extensively investigated, very few studies have been reported on transition-metal germanide NWs.[4a] Because the excitonic Bohr radius (24.3 nm) of bulk Ge is much larger than that (4.7 nm) of Si,[4b] the quantum size effect would be more prominent in transition-metal germanide NWs. Furthermore, the subtle change of the magnetic properties of iron germanides, varying sensitively with the composition ratio of Fe and Ge, has attracted much interest.[5] For example, hexagonal FeGe (B35 type of structure) is an antiferromagnet with a Neél temperature (T_N) of 411 K,[6a] hexagonal $Fe_{1.67}Ge$ ($B8_2$ type of structure) is ferromagnetic with a Curie temperature (T_c) of 485 K,[6b] and hexagonal $Fe_{1.4}Ge$ ($B8_2$ type of structure) in the η-phase is ferromagnetic with T_c of 270 K.[6c] The η-phase can be formed when Ge contents are between 40.8 and 43.5 atomic %. As the Ge composition increases, T_c decreases rapidly to ~200 K at 43.5 atomic %.[5]

The magnetic properties of nanoscale materials are strongly affected by the physical parameters such as the size and lattice constant.[3a,7,8] For example, ferromagnetism in Cu-doped GaN NWs was strongly enhanced as compared to bulk Cu-doped GaN,[2b] which was attributed to the reduction of the Cu t_d bandwidth due to the 1D nature.[9] Ferromagnetism was also stabilized by lattice compression in the nanophase of epitaxially grown monoclinic FeGe on Ge substrate, whereas an antiferromagnetic (AFM) ordering appears in the bulk.[7]

Herein, we report the results of both experimental and theoretical studies on the ferromagnetic stabilization of $Fe_{1.3}Ge$ NWs and their origin. Single-crystalline free-standing hexagonal $Fe_{1.3}Ge$ NWs were synthesized by a simple chemical vapor transport (CVT) process without using any catalyst. To the best of our knowledge, this is the first report on the synthesis of free-standing single-crystalline iron germanide NWs. Interestingly, these hexagonal $Fe_{1.3}Ge$ NWs exhibit T_c above 350 K,

[†] Department of Chemistry, KAIST.
[‡] Department of Physics, KAIST.
[§] KBSI.

(1) (a) Qian, C.; Kim, F.; Ma, L.; Tsui, F.; Yang, P.; Liu, J. *J. Am. Chem. Soc.* **2004**, *126*, 1195. (b) Falk, A. L.; Koppens, F. H. L.; Yu, C. L.; Kang, K.; de Leon Snapp, N.; Akimov, A. V.; Jo, M.-H.; Lukin, M. D.; Park, H. *Nat. Phys.* **2009**, *5*, 475. (c) Wu, B.; Heidelberg, A.; Boland, J. J. *Nat. Mater.* **2005**, *4*, 525.
(2) (a) Liang, W.; Yuhas, B. D.; Yang, P. *Nano Lett.* **2009**, *9*, 892. (b) Seong, H.-K.; Kim, J.-Y.; Kim, J.-J.; Lee, S.-C.; Kim, S.-R.; Kim, U.; Park, T.-E.; Choi, H.-J. *Nano Lett.* **2007**, *7*, 3366.
(3) (a) Seo, K.; Varadwaj, K. S. K.; Mohanty, P.; Lee, S.; Jo, Y.; Jung, M.-H.; Kim, J.; Kim, B. *Nano Lett.* **2007**, *7*, 1240. (b) Seo, K.; Lee, S.; Jo, Y.; Jung, M.-H.; Kim, J.; Kim, B. *J. Phys. Chem. C* **2009**, *113*, 6902. (c) van der Meulen, M. I.; Petkov, N.; Morris, M. A.; Kazakova, O.; Han, X.; Wang, K. L.; Jacob, A. P.; Holmes, J. D. *Nano Lett.* **2009**, *9*, 50. (d) Lensch-Falk, J. L.; Hemesath, E. R.; Lauhon, L. J. *Nano Lett.* **2008**, *8*, 2669.
(4) (a) Yoon, H.; Seo, K.; Bagkar, N.; In, J.; Park, J.; Kim, J.; Kim, B. *Adv. Mater.* **2009**, *21*, 4979. (b) Nguyen, P.; Ng, H. T.; Meyyappan, M. *Adv. Mater.* **2005**, *17*, 549.
(5) Kanematsu, K. *J. Phys. Soc. Jpn.* **1965**, *20*, 36.
(6) (a) Sundström, L. J. *Phys. Scr.* **1972**, *6*, 158. (b) Yasukōchi, K.; Kanematsu, K. *J. Phys. Soc. Jpn.* **1961**, *16*, 429. (c) Eliezer, D.; Nadiv, S.; Ron, M. *Appl. Phys. Lett.* **1975**, *26*, 340.
(7) Zeng, C.; Kent, P. R. C.; Varela, M.; Eisenbach, M.; Stocks, G. M.; Torija, M.; Shen, J.; Weitering, H. H. *Phys. Rev. Lett.* **2006**, *96*, 127201.
(8) Teng, X.; Feygenson, M.; Wang, Q.; He, J.; Du, W.; Frenkel, A. I.; Han, W.; Aronson, M. *Nano Lett.* **2009**, *9*, 3177.
(9) Xiang, H. J.; Wei, S.-H. *Nano Lett.* **2008**, *8*, 1825.

Scheme 1. Experimental Setup

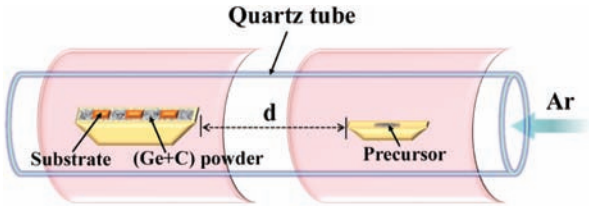

much higher than the bulk value of 200 K. We performed first-principles density functional calculations to investigate the enhanced ferromagnetic ordering in $Fe_{1.3}Ge$ NWs and also to study the effects of strain and low-dimensionality on the magnetic coupling in the NWs.

Free-standing hexagonal $Fe_{1.3}Ge$ NWs were synthesized in a hot wall dual-zone furnace via a CVT method (Scheme 1) without catalysts. The hexagonal $Fe_{1.3}Ge$ NWs were grown on a *c*-plane sapphire substrate (5 mm × 5 mm) placed on a powdered Ge/C mixture of 1:1 (weight ratio) Ge powder (Sigma-Aldrich, 99.999%) and graphite powder (Kanto chemical Co.). The Ge/C powder mixture was employed as a source for Ge. The furnace has an 1 in. diameter quartz tube. The upstream (US) and downstream (DS) zones were used for the vaporization of precursors and the nanostructure growth, respectively. An anhydrous FeI_2 powder (Sigma-Aldrich, 99.99%) in an alumina boat was placed at the center of the US zone. The substrate was placed at 20 cm (the *d* value in Scheme 1) from the precursor in the DS zone. Temperatures of the US and DS zones were maintained at 650 and 870 °C, respectively, during the reaction time of 10 min, while the pressure was maintained at 1 atm. The Ar flow rate was set to ∼200 sccm to synthesize hexagonal $Fe_{1.3}Ge$ NWs.

Field emission scanning electron microscope (FESEM) images of hexagonal $Fe_{1.3}Ge$ NWs were taken on a Phillips XL30S. X-ray diffraction (XRD) patterns of the specimen were recorded on a Rigaku D/max-rc (12 kW) diffractometer operated at 40 kV and 100 mA with the filtered 0.15405 nm $Cu_{K\alpha}$ radiation. Transmission electron microscope (TEM) images, high-resolution TEM (HRTEM) images, and selected area electron diffraction (SAED) patterns were taken on JEOL JEM-2100F TEM operated at 200 kV. Compositions of the $Fe_{1.3}Ge$ NWs were studied by X-ray energy-dispersive spectrometry (EDS). Electron energy-loss spectroscopy (EELS) measurements were performed on the TEM (JEOL JEM-2100F). The temperature and field dependences of the magnetization were measured by using a commercial superconducting quantum interference device (SQUID) magnetometer (Quantum Design, MPMS7).

Morphologies and elemental compositions of hexagonal $Fe_{1.3}Ge$ NWs were examined by SEM, TEM, and EDS. Figure 1a shows an SEM image of the NWs grown on a *c*-plane sapphire substrate. A high magnification SEM image (Figure 1b) reveals the hexagonal cross section of the sidewall facets along with a truncated pyramidal pointed tip of the NW, consistent with other hexagonal NWs such as ZnO, GaN, and $CrSi_2$.[10] Diameters of NWs ranging from 100 to 250 nm and lengths up to tens of micrometers are observed.

Figure 2a shows a low-resolution TEM image and a SAED pattern obtained from a hexagonal $Fe_{1.3}Ge$ NW. The SAED

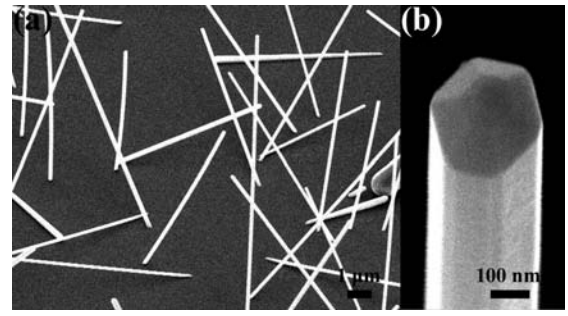

Figure 1. (a) SEM image of free-standing $Fe_{1.3}Ge$ NWs grown on a *c*-plane sapphire substrate. (b) High magnification SEM image of the tip of a NW, revealing a hexagonal cross section of the sidewall facets along with a pyramidal pointed tip.

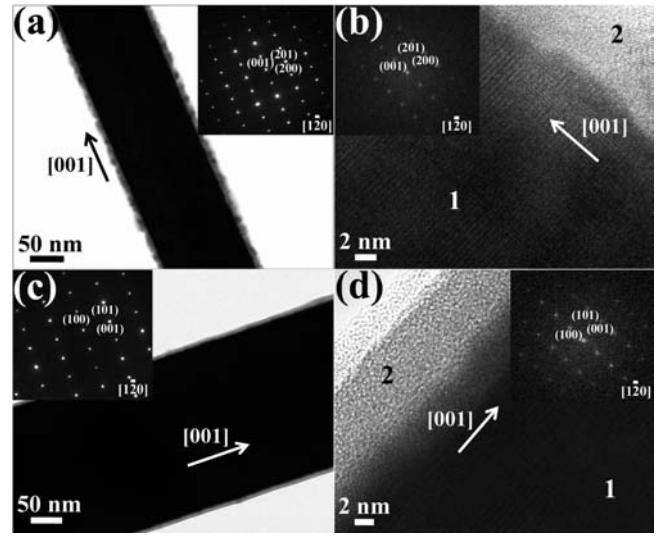

Figure 2. (a) TEM image and SAED pattern (inset) of a hexagonal $Fe_{1.3}Ge$ NW with a thin layer. (b) HRTEM image of a hexagonal $Fe_{1.3}Ge$ NW and its FFT (inset). (c) TEM image and SAED pattern (inset) of a hexagonal $Fe_{1.3}Ge$ NW after removing the thin layer. (d) HRTEM image of a hexagonal $Fe_{1.3}Ge$ NW after thin layer elimination and its FFT (inset).

pattern in the inset shows a regular spot pattern, reflecting single-crystalline nature of the NWs. The spots can be indexed to the hexagonal $Fe_{1.3}Ge$ structure (space group $P6_3/mmc$, JCPDS card no. 35-1182) down the $[1\bar{2}0]$ zone axis. The HRTEM image (Figure 2b) shows clear lattice fringes. Two-dimensional fast Fourier transform (FFT) (inset in Figure 2b) obtained from the HRTEM is also well matched to the hexagonal $Fe_{1.3}Ge$ structure, exhibiting the [001] growth direction of the NW. Note that the NW has thin surface layers with the thickness less than 10 nm. The EDS spectrum shows that the NW (region 1 in Figure 2b) consists of Fe and Ge in a ratio of 55:45 within 4% error, and the NW surface layer (region 2 in Figure 2b) consists of Fe and O (Supporting Information, Figure S1). EELS spectrum (Supporting Information, Figure S2a) exhibits two pronounced peaks at ∼709.7 and ∼722.4 eV, corresponding to the Fe-L_3 and Fe-L_2 edges, respectively. The Fe-L_2 and Fe-L_3 EELS data from the thin layers agree well with the reference values for wüstite (FeO) containing the divalent Fe^{2+} oxidation state.[11] In addition, the EELS analysis shows that the thin surface layers consist of Fe and O in a ratio of 1:1 within 8% error (Supporting Information, Figure S2b). We expect that the highly under-

(10) (a) Yoon, H.; Seo, K.; Moon, H.; Varadwaj, K. S. K.; In, J.; Kim, B. *J. Phys. Chem. C* **2008**, *112*, 9181. (b) Hersee, S. D.; Sun, X.; Wang, X. *Nano Lett.* **2006**, *6*, 1808. (c) Seo, K.; Varadwaj, K. S. K.; Cha, D.; In, J.; Kim, J.; Park, J.; Kim, B. *J. Phys. Chem. C* **2007**, *111*, 9072.

(11) Schmid, H. K.; Mader, W. *Micron* **2006**, *37*, 426.

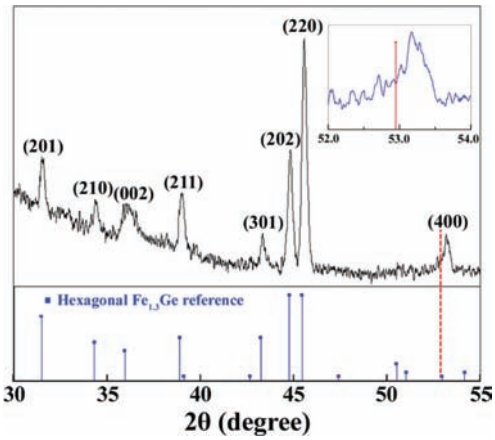

Figure 3. XRD patterns taken from the as-synthesized $Fe_{1.3}Ge$ NW ensemble. Inset shows the magnified (400) peak for a clear guide for the eye of the peak shift.

coordinated Fe atoms at the NW surface would undergo immediate oxidation on exposure to ambient, forming a FeO shell.

TEM (Figure 2c), HRTEM (Figure 2d), and TEM-EDS (Supporting Information, Figure S1c and S1d) analysis data were obtained from a representative hexagonal $Fe_{1.3}Ge$ NW after removing the FeO layers by etching in 1% H_2SO_4 solution for 6 h. No change is observed in the crystal structure and elemental composition of the $Fe_{1.3}Ge$ NW after etching.

Figure 3 shows the XRD pattern from the as-grown NW ensemble, in which the entire diffraction peaks match well with the hexagonal $Fe_{1.3}Ge$ structure (space group $P6_3/mmc$, JCPDS card no. 35-1182). No other phases are observed in the XRD data. A closer view of the XRD peak (inset in Figure 3) with the standard pattern (JCPDS # 35-1182) reveals that the (400) peak shifts slightly to a higher angle, suggesting that the NW is slightly compressed along the [100] direction.

The magnetic properties of the $Fe_{1.3}Ge$ NW ensemble after eliminating thin FeO layers were examined by a SQUID magnetometer. Figure 4a displays the temperature-dependent magnetization ($M-T$) curves measured under an applied magnetic field of 2000 Oe, after zero-field cooling (ZFC: ●) and field cooling (FC: blue ●), respectively. The $M-T$ curves show nonzero magnetization up to room temperature with similar FC and ZFC data. The field-dependent magnetization ($M-H$) curves at 5 and 300 K are shown in Figure 4b. The $M-H$ curves were obtained after correction for the diamagnetic component arising from the sapphire substrate. The two $M-H$ curves show clearly the hysteresis behavior both with the coercive field (H_c) of about 80 Oe. The hysteresis loops and the $M-T$ curves indicate that the as-synthesized NWs are ferromagnetic at room temperature, whereas the reported T_c of the bulk phase is ~200 K.[5] To investigate other contribution to magnetic hysteresis, such as superparamagnetism and spin glass, we have measured the time dependence of magnetization. There was no magnetic relaxation at 5 K and 1000 Oe up to 2 h (Supporting Information, Figure S3), confirming the ferromagnetism of the sample. The magnetic properties of the $Fe_{1.3}Ge$ NWs covered with thin FeO layers also reveal the ferromagnetic behavior (Supporting Information, Figure S4) with the T_c higher than room temperature. The surface effect on the ferromagnetism of $Fe_{1.3}Ge$ NWs would be rather small because their diameters are 100−200 nm.

We performed spin-polarized density functional calculations to investigate the magnetic coupling in hexagonal $Fe_{1.3}Ge$ NWs,

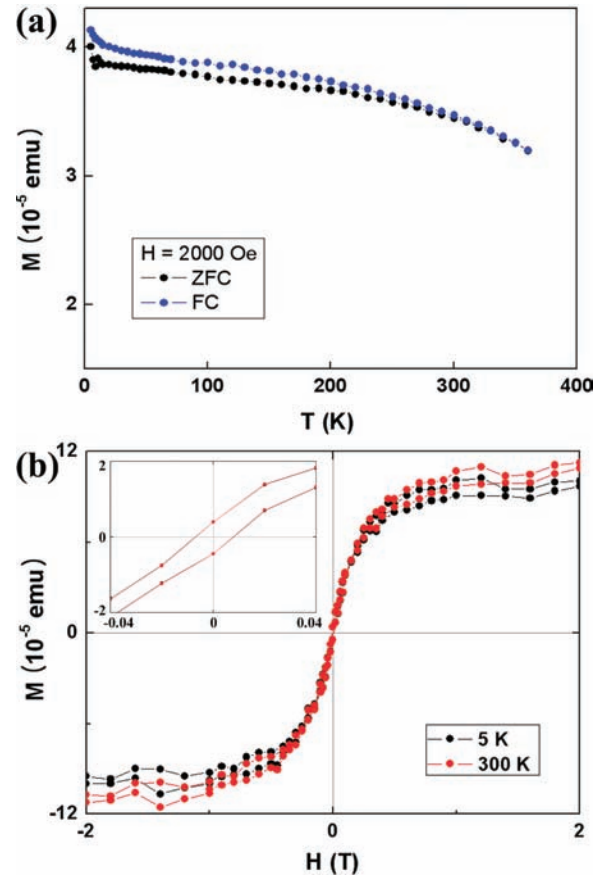

Figure 4. (a) Plot of M versus T for a $Fe_{1.3}Ge$ NW ensemble at an applied field of 2000 Oe. Black and blue "●" represent the ZFC and FC data, respectively. The $M-T$ curves indicate that the T_c is above room temperature. (b) Plot of M versus H for the $Fe_{1.3}Ge$ NW ensemble at 5 and 300 K, respectively. Inset shows the hysteresis loops on an enlarged scale.

using the generalized gradient approximation (GGA) for the exchange-correlation potential and the projector augmented wave (PAW) potentials,[12−15] as implemented in the VASP code.[16] For both bulk and NW systems, we employed plane waves up to a cutoff of 410 eV and k-points generated by the $4 \times 4 \times 3$ and $1 \times 1 \times 3$ Monkhorst−Pack meshes,[17] respectively, for Brillouin-zone integration. The NWs considered were oriented along the [001] direction, with diameters of about 12 Å, and neighboring wires were separated by 22 Å, including a vacuum region of 10 Å, which prohibits wire−wire interactions. All atomic positions were fully optimized until the residual forces on each atom were less than 0.05 eV/Å.

For the bulk, we considered the hexagonal η-phase,[5] with the lattice parameters set to the measured values, $a = b = 7.976$ Å and $2c = 9.986$ Å. In the unit cell of $Fe_{22}Ge_{17}$, 16 Fe and 16 Ge atoms were fixed at the lattice sites, whereas 2 Fe atoms were randomly positioned at 4 A sites, and 4 Fe and 1 Ge atoms were also randomly located at 12 B sites (Figure 5a and Supporting Information, Figure S5). Among many configurations available for the distribution of Fe and Ge, we chose 10 different configurations of bulk $Fe_{22}Ge_{17}$ and used them to

(12) (a) Hohenberg, P.; Kohn, W. *Phys. Rev.* **1964**, *136*, B864. (b) Kohn, W.; Sham, L. J. *Phys. Rev.* **1965**, *140*, A1133.
(13) Perdew, J. P.; Wang, Y. *Phys. Rev. B* **1992**, *45*, 13244.
(14) Blöchl, P. E. *Phys. Rev. B* **1994**, *50*, 17953.
(15) Kresse, G.; Joubert, D. *Phys. Rev. B* **1999**, *59*, 1758.
(16) Kresse, G.; Furthmüller, J. *Phys. Rev. B* **1996**, *54*, 11169.
(17) Monkhorst, H. J.; Pack, J. D. *Phys. Rev. B* **1976**, *13*, 5188.

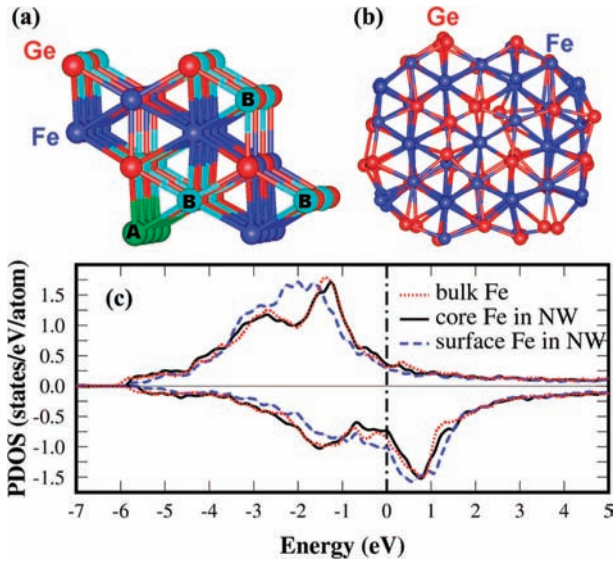

Figure 5. (a) Top view of the atomic structure of bulk $Fe_{22}Ge_{17}$ before 6 Fe and 1 Ge atoms are distributed randomly among available A and B sites. (b) Top view of the relaxed atomic structure of a single $Fe_{66}Ge_{51}$ NW showing one of 10 calculated configurations for the distribution of Fe and Ge. (c) The PDOS onto the Fe atoms of the bulk (red dotted lines) and onto the core (black solid lines) and surface (blue dashed lines) Fe atoms in the NW. The vertical line denotes the Fermi level set to zero.

generate $Fe_{66}Ge_{51}$ NWs. All the physical properties of bulk and NW systems were obtained by taking an average over these configurations. The NW consisting of 66 Fe and 51 Ge atoms (Figure 5b) satisfies well the stoichiometry of synthesized $Fe_{1.3}Ge$ NWs. In the bulk, the Fe atoms are bonded to 5.02 Fe and 5.09 Ge atoms, with an average coordination number of 10.11, and the average Fe−Fe and Fe−Ge bond lengths are 2.58 and 2.55 Å, respectively. In the NW, the lattice parameters a and b were optimized with a fixed axial lattice constant, and all the atoms were relaxed. The core Fe atoms have an average coordination number of 10.15, bonding with 5.08 Fe and 5.07 Ge atoms. The average bond length is 2.54 Å for both Fe−Fe and Fe−Ge bonds, being slightly reduced as compared to the bulk. On the NW surface, the Fe coordination number is considerably reduced to 7.39, with 3.74 Fe−Fe and 3.65 Fe−Ge bonds. Because of large relaxations of the under-coordinated Fe atoms, the average bond lengths of the Fe−Fe and Fe−Ge bonds decrease to 2.51 and 2.49 Å, respectively, close to the bulk value of 2.48 Å for bcc α-Fe.[18]

For the $Fe_{66}Ge_{51}$ NW, the total density of states and the projected density of states (PDOS) onto the Fe atoms in the ferromagnetic (FM) state are compared to those for bulk $Fe_{66}Ge_{51}$ in Figure 5c and Figure S5 (Supporting Information). The PDOS onto the core Fe atoms exhibits two well-separated peaks that represent the bonding and antibonding d states. Although these peaks resemble those of the bulk, the bandwidth is slightly reduced. For the surface Fe atoms, hybridization of the Fe d orbitals is weakened because of the lower coordination number. Separation between the bonding and antibonding states is reduced, leading to a broadened peak between the bonding and antibonding peaks and a larger exchange splitting. In $(Fe_xCo_{1-x})_{1.67}Ge$ systems, it was reported that T_c increases with decreasing Co content due to the increased number of Fe−Fe bonds.[19] Similarly, when the Ge content decreases in $Fe_{1+x}Ge$ systems ($0.3 \leq x \leq 0.85$), the saturation magnetization and T_c were shown to be enhanced.[5] The Fe magnetic moment tends to increase as the number of the surrounding Ge atoms decreases, because the p−d hybridization is suppressed.

For bulk $Fe_{22}Ge_{17}$, the FM state is found to be the ground state, with an average energy lower by about 74 meV per Fe atom than the AFM state. In the AFM spin configuration, the Fe atoms on the same hexagonal plane tend to have the same spins. In the supercell, two types of the hexagonal layers containing only Fe atoms or a mixture of the Fe and Ge atoms are alternately stacked along the c-axis (Figure 5a). Thus, spin-up and spin-down layers are repeated after two consecutive layers in the AFM state with vanishing remnant magnetic moments. For the NW, of which $Fe_{66}Ge_{51}$ structure is employed, ferromagnetic stability is enhanced, with an average energy difference (ΔE) of about 90 meV per Fe atom between the FM and AFM states. In some AFM configurations of the NW system, spin-up and spin-down layers are not well-defined due to much larger relaxations than the bulk, giving finite remnant magnetic moments and smaller energy differences. When these not-well-defined configurations are excluded, ΔE is obtained as 100 meV per Fe atom. Although ΔE is little smaller than what is expected from the experimentally observed ferromagnetic enhancement making T_c higher than room temperature, our calculations clearly indicate that the ferromagnetic stability is significantly enhanced in the NW as compared to the bulk, which is consistent with the experimental observation.

The stronger ferromagnetic coupling in the NW is attributed to stronger interaction between the Fe atoms due to the enhanced magnetic moment per Fe atom and increased number of Fe−Fe bonds than that in the bulk. Calculated average magnetic moments per Fe atom in the $Fe_{66}Ge_{51}$ NW system are 1.80 and 2.26 μ_B for the core and the surface Fe atoms, respectively. The magnetic moment for the bulk is calculated as 1.75 μ_B per Fe atom. To derive the Fe magnetic moment (μ_{Fe}) from the saturation magnetization (M_s) in the $M-H$ curve, we first measured the total volume of $Fe_{1.3}Ge$ NWs and then obtained the total mass. In the synthesized $Fe_{1.3}Ge$ NW ensemble, using the measured value of $M_s = 63$ emu/g at 5 K, we estimate the maximum magnetic moment to be 1.3 μ_B (± 0.5) per Fe atom (see the Supporting Information). These M_s and μ_{Fe} values are much larger than those previously reported for bulk $Fe_{1.3}Ge$, $M_s \approx 40$ emu/g and $\mu_{Fe} \approx 0.8\ \mu_B$ per Fe atom at 0 K,[5] indicating ferromagnetic enhancement. Although the calculated magnetic enhancement for the NW is not as much as observed in the experiment, the calculation estimates correctly that the magnetic moment is enhanced in the NW as compared to the bulk.

Because crystalline $Fe_{1.3}Ge$ is a very unique material that has lots of vacancies, the coordination numbers show large fluctuations. The structural relaxations induced by these vacancies can be even larger for the $Fe_{1.3}Ge$ NW due to strong influence imposed by the NW surface. The number of Fe−Fe bonds is 5.08 ± 0.21 in the core region of $Fe_{1.3}Ge$ NWs and 5.02 ± 0.08 in bulk $Fe_{1.3}Ge$. Larger standard deviation for the NW than for bulk indicates that the NW can have more Fe atoms having larger numbers of Fe−Fe bonds and thus contributing much to the ferromagnetism. Recently, it was reported that Fe coordination number is highly important in the ferromagnetism of Fe_xGe_y

(18) Shabanova, I. N.; Kormilets, V. I.; Zagrebin, L. D.; Terebova, N. S. *J. Struct. Chem.* **1998**, *39*, 904.

(19) Kanematsu, K.; Yasukōchi, K.; Ohoyama, T. *J. Phys. Soc. Jpn.* **1963**, *18*, 1429.

alloys.[20] In our calculation, NW configurations in which Fe atoms are locally gathered together have larger ΔE values than those having relatively well-distributed Fe atoms. The Fe magnetic moment is also large for these locally gathered Fe atoms. Thus, the large deviation in the Fe coordination number due to the more relaxed structure in the NW seems to contribute to the enhanced ferromagnetism in the $Fe_{1.3}Ge$ NW. Our calculated ΔE between FM and AFM states includes all these factors, showing significantly increased ΔE of 100 meV for the NW as compared to that of bulk, 74 meV.

Finally, we examine the effect of compressive and tensile strain on the magnetic stability. The magnetic interactions between the Fe atoms can be affected by their relative distances. For strained monoclinic FeGe NWs, recent experiments and theoretical calculations showed that lattice compression as much as a few angstroms destabilizes the AFM ground state and induces the ferromagnetism.[7] The shift of the (400) peak to a higher angle (Figure 3) in the XRD spectrum is thought to be related to the lattice compression along the [100] axis. When the lattice parameter *a* or *b* decreases or increases by 0.1 Å in the bulk, the ferromagnetic stability is enhanced by less than 1 meV per Fe atom. Although for as-synthesized hexagonal $Fe_{1.3}Ge$ NWs the (100) lattice parameter of the $Fe_{1.3}Ge$ NW was estimated to be 6.868 Å with a lattice compression of only about 0.04 Å as compared to the bulk value of 6.912 Å, the strain effect partly accounts for the enhanced ferromagnetism in the NW. More comprehensive calculations are required to determine the complete map for ΔE, varying the lattice parameters, which is beyond the scope of the present work.

The composition ratio of iron germanide NWs can be controlled by adjusting experimental conditions, such as the amounts of FeI_2 and Ge powders and precursor heating temperature. Hexagonal Fe_3Ge NWs were synthesized using a smaller amount of Ge precursor and the higher temperature for the FeI_2 vaporization to increase Fe vapor pressure (Supporting Information, Figures S6−S8). Further experiments to grow iron germanide NWs with various composition ratios and to investigate their magnetic properties are currently underway.

In conclusion, we have successfully grown single-crystalline free-standing $Fe_{1.3}Ge$ NWs with the hexagonal $B8_2$ type crystal structure on a *c*-plane sapphire substrate using a CVT process. As-grown hexagonal $Fe_{1.3}Ge$ NWs have shown room temperature ferromagnetism, with the T_c much increased from 200 K of bulk hexagonal $Fe_{1.3}Ge$. First-principle density functional calculations for the $Fe_{66}Ge_{51}$ NW showed that the core Fe atom bonds with a larger number of the Fe atoms, with the average Fe−Fe distance smaller than that of the bulk. Both calculated and measured magnetic moments per Fe atom are larger than those of the bulk, leading to the stronger exchange interaction. We suggest that the enhanced ferromagnetism in synthesized $Fe_{1.3}Ge$ NWs is attributed to the increased ferromagnetic coupling between the magnetic Fe atoms. The ferromagnetic stability was also found to be slightly enhanced under strain. Furthermore, the stoichiometry of iron germanide NWs can be controlled by adjusting experimental conditions. The free-standing $Fe_{1.3}Ge$ NWs with room temperature ferromagnetism could be a good candidate as building blocks for practical nanospintronic devices.

Acknowledgment. This research was supported by NRF through NRL (2010-0018868), SRC (2010-0001484), and the "Center for Nanostructured Material Technology" under the "21st Century Frontier R&D Programs" (2010-K000350) of the MEST, Korea. SEM and TEM analyses were performed at the KBSI in Daejeon. E.-A.C. and K.J.C. acknowledge the support by the NRF (2009-0093845). The work of Y.J. was supported by KBSI grant (T30405).

Supporting Information Available: TEM-EDS spectra, EELS spectrum, additional SQUID data for as-grown $Fe_{1.3}Ge$ NWs, atomic and electronic structures of bulk and NW systems of FeGe, measurements of saturated magnetic moment, and synthesis of Fe_3Ge NWs. This material is available free of charge via the Internet at http://pubs.acs.org.

JA104189P

(20) Jaafar, R.; Berling, D.; Sébilleau, D.; Garreau, G. *Phys. Rev. B* **2010**, *81*, 155423.